

# Dynamic geomagnetic rigidity cutoff variations during a solar proton event

Craig J. Rodger

Department of Physics, University of Otago, Dunedin, New Zealand

Mark A. Clilverd

Physical Sciences Division, British Antarctic Survey, Cambridge, United Kingdom

Pekka T. Verronen

Finnish Meteorological Institute, Helsinki, Finland.

Thomas Ulich

Sodankylä Geophisica Observatory, Sodankylä, Finland.

Martin J. Jarvis

Physical Sciences Division, British Antarctic Survey, Cambridge, United Kingdom

Esa Turunen

Sodankylä Geophysical Observatory, Sodankylä, Finland.

**Abstract.** Solar Proton Events (SPE) are major, though infrequent, space weather phenomena that can produce hazardous effects in the near-Earth space environment. A detailed understanding of their effects depends upon knowledge of the dynamic rigidity cutoffs imposed by the changing total magnetic field. For the first time we investigate detailed comparisons between theoretical cutoff rigidities and ground-based measurements during the large geomagnetic disturbance of 4-10 November 2001. We make use of the imaging riometer (IRIS) at Halley, Antarctica, fortunately situated such that the rigidity cutoff sweeps back and forth across the instrument's field of view during the SPE period. The  $K_p$ -dependent geomagnetic

rigidity cutoff energies are determined from satellite observations combined with previously reported particle-tracing results. We find that the predicted absorption levels show good agreement with those experimentally observed for low and mid levels of geomagnetic disturbance ( $K_p < 5$ ). However, during more disturbed geomagnetic conditions the cutoff modeling over-estimates the stretching of the geomagnetic field, under-estimating the rigidity cutoff energies, and hence leading to riometer absorption predictions that are too high. In very disturbed conditions ( $K_p \approx 7-9$ ) the rigidity energy cutoffs indicated by the IRIS observations appear to be equivalent to those predicted for  $K_p \approx 6$  by the particle-tracing approach. Examples of changing rigidity cutoff contours for increasing levels of geomagnetic disturbance are presented.

## 1. Introduction

Processes on the Sun can accelerate protons to relativistic energies, producing Solar Proton Events (SPE), also known as Solar Energetic Particle (SEP) events. Arguments continue as to whether the acceleration is driven by the X-ray flare release process or in solar wind shock fronts during coronal mass ejections [Krucker and Lin, 2000; Cane *et al.*, 2003]. The high-energy component of this proton population is at relativistic levels such that they can reach the Earth within minutes of solar X-rays produced during any solar flares which may be associated with the acceleration. Satellite data show that the protons involved have an energy range spanning 1 to 500 MeV, occur relatively infrequently, and show high variability in their intensity and duration [Shea and Smart, 1990]. For large events the duration is typically several days, with risetimes of  $\sim 1$  hour, and a slow decay to normal flux values thereafter [Reeves *et al.*, 1992].

The most energetic SPE population deposits its energy at altitudes as low as 20-30 km, producing ionization and changing the local atmospheric chemistry. SPE particles generally lie at energies below which nuclear interaction-losses will be significant, such that ionization-producing atmospheric interactions are the dominant energy loss. Particle precipitation results in

enhancement of odd nitrogen ( $\text{NO}_x$ ) and odd hydrogen ( $\text{HO}_x$ ).  $\text{NO}_x$  and  $\text{HO}_x$  play a key role in the ozone balance of the middle atmosphere because they destroy odd oxygen through catalytic reactions [e.g., *Brasseur and Solomon*, 1986, pp. 291-299]. SPE-produced ionization changes tend to peak at  $\sim 70$  km altitude [*Clilverd et al.*, 2005a], leading to local perturbations in ozone levels [*Verronen et al.*, 2005]. While the ozone destruction at such high altitudes is generally not important to the total ozone population, under some conditions  $\text{NO}_x$  can be long-lived, particularly during polar winter at high latitudes. In this situation vertical transport can drive the  $\text{NO}_x$  down towards the large ozone populations in the stratosphere, leading to large long-lived ozone depletions [e.g., *Reid et al.*, 1991]. Changes in  $\text{NO}_x$  and  $\text{O}_3$  consistent with SPE-driven modifications have been observed [*Seppälä et al.*, 2004, *Verronen et al.*, 2005], and large depletion in ozone during the Arctic winter have been associated with a series of large SPEs over the preceding months [*Randall et al.*, 2005].

SPE particles cannot, however, access the entire global atmosphere as they are partially guided by the geomagnetic field. The first description of cosmic rays in the Earth's magnetic field [*Störmer*, 1930] demonstrated the geomagnetic cutoff rigidity, the minimum rigidity a particle must possess to penetrate to a given geomagnetic latitude, where the rigidity of a particle is defined as the momentum per unit charge. Therefore, every geomagnetic position has a corresponding cutoff rigidity. Higher rigidities are required to reach lower geomagnetic latitudes, and thus all particles with rigidities larger than the minimum can penetrate to that latitude (and all higher latitudes). In general the geomagnetic cutoff rigidity of a particle is also a function of its direction of arrival. While this effect was initially modeled with a static dipole field, the geomagnetic cutoff rigidity is a much more dynamic quantity depending on the Earth's internal and external magnetic fields. As such the geomagnetic cutoff varies spatially and with time, on timescales of both the internal (years) [*Smart and Shea*, 2003b] and the external field (minutes-hours) [*Kress et al.*, 2004].

Experimental measurements of geomagnetic cutoff rigidities have generally been based on satellite observations, while theoretical calculations have primarily focused on tracing particles through models of the Earth's field producing grids of estimated cutoff rigidities distributed over the Earth at a given altitude [e.g., *Smart and Shea*, 1985]. Comparisons between satellite-derived rigidity cutoffs and those determined by particle tracing studies generally show the measured cutoff latitudes are several degrees lower than the theoretical values [e.g., *Fanselow and Stone*, 1972]. However, new calculations undertaken using improved geomagnetic field models have resulted in lower rigidity-determined latitude cutoffs than earlier particle tracing studies [e.g., *Smart et al.*, 2003a], improving this comparison.

Generally, the satellite-derived cutoff rigidities have neglected the dynamic nature of the magnetic field, by considering the average magnetic field configuration present over a long time period [e.g., *Ogliore et al.*, 2001] or for a relatively fixed disturbance level (i.e., a fixed  $K_p$  value) during a short time period [e.g., *Dyer et al.*, 2003]. Due to the low-orbital altitudes of most of the satellites involved, few experimental studies have derived cutoffs during the most disturbed conditions during geomagnetic storms. One example, however, is the injection and formation of a new proton population in the inner radiation belt triggered by a large solar wind density enhancement compressing the cutoff rigidities for the 23-24 November 2001 storm [*Kress et al.*, 2004]; here the dynamic modeling of the cutoff values lead to additional understanding of SPE particle access to the inner magnetosphere.

As noted above, the impact of SPE particles upon the upper atmosphere leads to significant additional ionization, which can be detected through ground-based observations. The ionospheric effects of SPEs were first identified through the large absorption increases in VHF communications during the 23 February 1956 event [*Bailey*, 1957]. Long-range remote sensing of SPE-produced ionospheric modifications has been undertaken by examining the phase and amplitude changes of LF and VLF transmissions propagating beneath the ionosphere [e.g.,

*Westerlund et al.*, 1969]. Recent studies have contrasted calculated electron density profiles output from a SPE-driven atmospheric chemistry model with radio propagation observations, particularly for the 4-10 November 2001 [*Clilverd et al.*, 2005a] and October/November 2003 storms [*Verronen et al.*, 2005; *Clilverd et al.*, 2005b]. These studies have shown that our understanding of VLF propagation influenced by SPEs is high, such that VLF observations might be used to predict changes in the ionospheric D-region electron density profiles during other particle precipitation events. However, observations of subionospheric propagation of long wavelength electromagnetic waves are not well-suited for determining geomagnetic cutoff rigidities. While studies have shown these techniques are well-suited for testing ionospheric modification profiles [e.g., *Clilverd et al.*, 2005a], even short paths partially affected by SPE ionization are dominated by the altered ionosphere. During the October/November 2003 SPEs, the path from a transmitter in Iceland to a receiver in Erd, Budapest was modeled by applying a SPE-modified ionosphere to the first 500 km of the ~3000 km path [*Clilverd et al.*, 2005b]. The propagation modeling showed remarkably good agreement with the SPE-influenced data, despite the small percentage of the path which will have been affected by the SPE precipitation.

In contrast, riometers (relative ionospheric opacity meter), which measure the absorption of cosmic radio noise at a given frequency (usually 20-40 MHz) provide essentially overhead measurements of ionization levels, and are well suited for examining geomagnetic cutoffs. This is particularly true for imaging riometer systems (IRIS) where large receiver arrays provide an image of the ionospheric absorption levels above the instrument [*Detrick and Rosenberg*, 1990]. It has been shown that there is an empirical relationship between the square root of the integral proton flux (>10 MeV) and cosmic noise absorption (CNA) in daytime, at least when geomagnetic cutoff effects do not limit the fluxes [*Kavanagh et al.*, 2004]. The same study concluded that variations in the spectral hardness of the SPE proton flux and atmospheric collision frequencies do not cause significant departures from the linear relationships observed.

SPEs are major, though infrequent, space weather phenomena that can produce hazardous effects in the near-Earth space environment. The occurrence of SPE during solar minimum years is very low, while in active Sun years, especially during the falling and rising phases of the solar cycle, SPEs may average one per month. The impacts of SPEs include 'upsets' experienced by Earth-orbiting satellites, increased radiation exposure levels for humans onboard spacecraft and high-altitude aircraft, ozone depletions and disruption to HF/VHF communications in mid- and high-latitude regions. A detailed understanding of all these impacts depends upon knowledge of the dynamic rigidity cutoffs imposed by the changing total magnetic field. A number of studies have determined cutoff rigidities from spacecraft dose applications on the basis of theoretical calculations. However, to the best of our knowledge, the studies by *Smart and Shea* [2001] were the first to calculate dynamic vertical cutoff rigidities using the magnetic-activity level dependent Tsyganenko magnetospheric field model [*Tsyganenko*, 1989].

In this paper we make use of the conclusions of Smart and Shea to examine ground-based measurements depending upon the varying rigidity cutoffs during an SPE event. A case study using data from 4-10 November 2001 is undertaken based on the observations from an imaging riometer at Halley, Antarctica, fortunately situated such that the rigidity cutoff sweeps back and forth across the instrument's field of view during the SPE period. Thus for the first time we investigate detailed comparisons of theoretical cutoff rigidities and ground-based measurements during a large geomagnetic disturbance.

## **2. Geophysical Conditions and Experimental Setup**

### **2.1 4-10 November 2001 SPE**

For the solar proton event of 4-10 November, 2001, the peak proton flux was  $31,700 \text{ cm}^{-2}\text{sr}^{-1}\text{s}^{-1}$  for proton energies  $>10 \text{ MeV}$  (i.e., 31,700 proton flux units, or pfu). Figure 1 shows the integral unidirectional proton flux measurements reported by the geostationary GOES-8 satellite (upper

panel) during this SPE. The event started with a sudden increase in particle flux at about 16 UT on 4 November, 2001, reaching high levels by 18 UT, and remaining high until the end of 5 November, and thereafter taking several more days to return back to pre-storm levels. Note that the high-energy SPE particle fluxes decay significantly faster than at lower energies (particularly the channels from  $>10$  MeV and below). The levels of geomagnetic activity showed a delayed increase from the start of the SPE (Figure 1, lower panel), with disturbed  $K_p=5$  conditions only occurring late on 5 November, before peaking at  $K_p=9^-$  early on 6 November. We analyse this event in part because of the significance of the large fluxes involved, but primarily because of the large range of geomagnetic disturbance ( $K_p$ ) levels which occur during the SPE, allowing an examination of the geomagnetic rigidity conditions. The ionospheric changes associated with this SPE have been examined by VLF subionospheric propagation [Clilverd *et al.*, 2005a], and through OSIRIS/Odin satellite observations [A. Seppälä, manuscript in preparation, 2005].

## 2.2 Riometer Measurements

The riometer utilizes the absorption of cosmic radio noise by the ionosphere [Little and Leinbach, 1959] to measure the enhancement of D-region electron concentration by energetic charged particle precipitation [Stauning, 1996]. The riometer technique compares the strength of the cosmic radio noise signal received on the ground to the normal sidereal variation referred to as the quiet-day curve (QDC) to produce the cosmic noise absorption (CNA). The instantaneous ionospheric absorption in decibels is derived from the ratio of the prevailing signal level to this curve [Krishnaswamy *et al.*, 1985]. In typical operations the absorption peaks near 90 km altitude, where the product of electron density and neutral collision frequency maximizes. In this paper we consider experimental observations from a riometer located at Halley (75.6°S, 26.32°W,  $L=4.6$ ), as shown in Figure 2.

At Halley the system is a snow-buried 49-beam imaging riometer, operating at 38.2 MHz and sampled every 1 sec [Rose *et al.*, 2000]. Several receivers are multiplexed through a phased array

of 64 crossed-dipole antennas to achieve narrow beam scanning of the D region. The beam width is  $13^\circ$ . In the meridian plane the most equatorward and poleward beams intersect the D region ionosphere about  $1^\circ$  north (equatorward) and south (poleward) from the vertical central beam, respectively [Jarvis *et al.*, Fig. 1, 2003]. Absorption values for obliquely orientated (non-vertical) beams are automatically corrected to vertical following the technique described by Hargreaves and Jarvis [1986].

### 3. Sodankylä Ion Chemistry Model

The Sodankylä Ion Chemistry (SIC) model is a 1-D chemical model designed for ionospheric D-region studies, solving the concentrations of 63 ions, including 27 negative ions, and 13 neutral species at altitudes across 20–150 km. Our study made use of SIC version 6.6.0. The model has recently been discussed by Verronen *et al.* [2005], building on original work by Turunen *et al.* [1996] and Verronen *et al.* [2002]. A detailed overview of the model was given in Verronen *et al.* [2005], but we summarize in a similar way here to provide background for this study. The SIC model was originally developed to calculate riometer absorptions, and has been successfully applied in the past [e.g., Turunen, 1993].

In the SIC model several hundred reactions are implemented, plus additional external forcing due to solar radiation (1–422.5 nm), electron and proton precipitation, and galactic cosmic radiation. Initial descriptions of the model are provided by Turunen *et al.* [1996], with neutral species modifications described by Verronen *et al.* [2002]. Solar flux is calculated with the SOLAR2000 model (version 2.21) [Tobiska *et al.*, 2000]. The scattered component of solar Lyman- $\alpha$  flux is included using the empirical approximation given by Thomas and Bowman [1986]. The SIC code includes vertical transport [Chabrilat *et al.*, 2002] which takes into account molecular [Banks and Kockarts, 1973] and eddy diffusion with a fixed eddy diffusion coefficient profile which has a maximum of  $1.3 \times 10^6 \text{ cm}^2 \text{ s}^{-1}$  at 102 km. The background neutral

atmosphere is calculated using the MSISE-90 model [Hedin, 1991] and tables given by Shimazaki [1984]. Transport and chemistry are advanced in intervals of 5 or 15 minutes. While within each interval exponentially increasing time steps are used because of the wide range of chemical time constants of the modeled species.

### 3.1 Proton Forcing

Here we use the SIC model to produce lower ionospheric electron density profiles in the winter-time D region generated above the Halley Bay IRIS instrument during the SPE over 4-10 November 2001. We start with the experimentally observed proton flux spectra reported by GOES-borne instruments at geosynchronous altitude (Fig. 1) and assume that the proton spectra at the top of the atmosphere will be determined only by these fluxes. In previous studies the magnetic latitudes were high enough to assume the proton flux spectra at the top of the atmosphere was the same as that reported by GOES [e.g., Verronen *et al.*, 2005; Clilverd *et al.*, 2005b], as the geomagnetic cutoff energy is zero for sufficiently high magnetic latitudes. The angular distribution of the protons is assumed to be isotropic over the upper atmosphere, which is valid close to the Earth [Hargreaves, 1992]. A SIC modeling run has also been undertaken without any proton forcing (i.e., zero proton fluxes), reasonable at Halley for low  $K_p$  conditions. The results of the no-forcing "control" SIC-run allow the calculation of "quiet-time" conditions.

Each run of the SIC model is based on a neutral background atmosphere given by MSISE-90 and provides concentration profiles of neutral and ionic species. Following Banks and Kockarts [1973; Part A, p. 194], we calculate the electron collision frequencies of  $N_2$ ,  $O_2$ , and He from MSIS and of O and H from SIC using the neutral temperature profile of MSIS, which we can assume to be equal to electron temperature below 100 km. Electron density is obtained from SIC by subtracting the sum of negative ion concentrations from the sum of positive ion concentrations. Finally, we use the method of Sen and Wyller [1960] to compute differential absorption  $dL/dh$  and integrate with respect to height. This method takes the operational

frequency of the riometer into account and assumes a dipole approximation for the geomagnetic field to obtain the electron gyrofrequency at the respective altitude and latitude.

## 4. Event Modeling and Observations

### 4.1 Riometer data and SIC calculated absorption

Figure 3 (left panel) shows the experimentally-observed cosmic noise absorptions reported by the meridional beams of the Halley IRIS instrument (i.e., pointing N-S) during the 4-10 November 2001 SPE with 15 min averaging. CNA are shown for IRIS beam 4 (overhead of Halley), the northernmost beam 7 (which we term the "equatorward beam"), and the southernmost beam 1 (which we term the "poleward beam"). As noted above, the "edge" beams map to the ionosphere so as to be viewing  $\sim 1^\circ$  north and south in latitude (i.e.  $75.6^\circ\text{S} \pm 1^\circ$ ). The right panel of Figure 3 shows the experimental relationship between the square root of the GOES-8 integral proton flux ( $>10$  MeV) and the Halley IRIS CNA observations, where the color of the data-marker is the same as the left panel. The numbers used to mark each data point is the rounded  $K_p$  value appropriate for that 15 min period. Included on this plot are the Halley IRIS overhead CNAs predicted from Sodankylä Ion Chemistry model calculations (described below), on the assumption that geomagnetic cutoff effects do not limit the fluxes. Clearly, the IRIS observations do not show the reported empirical linear relationship between the square root of the integral proton flux ( $>10$  MeV) and CNA [Kavanagh *et al.*, 2004], whereas the SIC absorption values do follow this relationship despite being determined from first principles. We therefore conclude that the response of the ionosphere above Halley is significantly influenced by rigidity cutoffs. We therefore can make use of the Halley IRIS data to test our ability to predict dynamic rigidity cutoffs and their variation during a severe geomagnetic storm.

### 4.2 Estimates of Rigidity Cutoffs

It has been recognized for some time that geomagnetic rigidity cutoffs are well-organized in terms of the McIlwain  $L$ -parameter [Smart and Shea, 1994; Selesnick *et al.*, 1995]. The  $L$ -

variation of the geomagnetic rigidity cutoff has been determined for quiet times from  $\approx 10,000$  nuclei observations made by the MAST instrument on the SAMPEX satellite [Ogliore *et al.*, 2001]. These authors report that the geomagnetic rigidity cutoffs,  $R_c$ , for quiet times are given by

$$R_c = 15.062 L^{-2} - 0.363 \quad (\text{in GV}) \quad (1)$$

representing average conditions for  $K_p=2.3$ . As noted above, dynamic vertical cutoff rigidities dependent upon magnetic activity levels have been determined by particle-tracing [Smart and Shea, 2003a] using the  $K_p$ -dependent Tsyganenko magnetospheric field model. These authors have reported that the change of proton cutoff energy with  $K_p$  is relatively uniform over the range of the original Tsyganenko (1989) model ( $K_p < 5$ ), but the cutoff changes introduced by the Boberg [1995] extension to higher  $K_p$  is non-linear such that there are large changes in proton cutoff energy for a given  $L$ -value at large  $K_p$  values. We make use of the  $K_p$ -dependent variations in the effective vertical cutoff energies at a given IGRF  $L$ -value at 450 km altitude determined from this modeling [Smart *et al.*, Fig. 5, 2003], but with a slight modification to ensure that the geomagnetic rigidity cutoff varies as  $15.062 L^{-2}$ , as observed in the SAMPEX experimental data. The results are presented in Figure 4. Note that the change in cutoff energy with geomagnetic activity is strongly non-linear at the highest disturbance levels. In order to interpolate down to lower altitudes (e.g., 100 km), we follow the approach outlined by Smart and Shea [2003a] again using the IGRF determined  $L$ -value. This exploits the basic relationship between  $R_c$  and  $L$ , i.e.,

$$R_c = V_k L^{-2} \quad (2)$$

where  $V_k$  is an altitude independent constant. Thus by knowing the value of  $V_k$  for the IGRF  $L$ -value at 450 km altitude above a given location, one can determine  $R_c$  at 100 km once one knows the  $L$ -value for that location at 100 km altitude. Time varying geomagnetic cutoff energy determined from this process is shown in Figure 5, for the location of the Halley IRIS viewing region (the IGRF invariant latitude of Halley is  $\sim 62.1^\circ$ ). Note the large differences in cutoff

energy for the poleward and equatorward IRIS beams, located only  $\sim 2^\circ$  apart in latitude, and that all beams drop to a zero cutoff energy when the  $K_p$  reaches its most disturbed levels.

#### 4.3 Middle Atmosphere Response to the 4-10 November 2001 SPEs

In order to calculate the SPE effects, we assume that the proton spectra leading to ionization detected by the IRIS instrument will be determined by GOES reported fluxes including only those particles with energies greater than the rigidity cutoff energy at 100 km, as estimated above. This is the first application of geomagnetic rigidity cutoffs to the SIC model. The response of the electron number density in the middle atmosphere to the 4-8 November 2001 SPE event as determined by the SIC model are presented in Figure 6. The uppermost panel in this figure shows the expected electron density directly overhead of Halley for a no-rigidity cutoff case (i.e., the impact of the GOES recorded fluxes at all energies). This should be contrasted with the next panel down, which shows the time-varying electron densities calculated for the same location, but where the SPE fluxes were modified by the dynamic geomagnetic cutoff energy thresholds (calculated in Section 4.2).

There are large differences in the electron density between the two upper panels, particularly at altitudes between  $\sim 50$ -90 km where the cutoff protons would otherwise have deposited their energy. Around 6 November 2001, when the  $K_p$  peaks and the cutoff energy threshold drops to zero (shown by a white bar), the two panels are essentially identical. The lower two panels show the ratio of the electron densities of the equatorward and poleward IRIS beams to the electron densities shown in the second panel (middle beam). The largest differences are between the equatorward and over-head IRIS locations, as there are significant differences between the geomagnetic cutoff energies at most times. The calculated electron densities in all panels of Figure 6 are essentially the same for the times where the  $K_p$  reaches its highest values, because the modeled cutoff energies drop to zero (Figure 5) for all the IRIS beam locations.

## 5. Estimates of IRIS absorption

### 5.1 Modeling the Halley IRIS observations

Figure 7 shows a comparison between the experimentally observed Halley IRIS riometer CNA (heavy line) and the absorptions calculated using the SIC model with dynamic geomagnetic rigidity cutoffs (light-gray line). The three panels contrast the absorption in the three IRIS beam directions, from the equatorward (North) to poleward (South) edges of the IRIS view. The middle panel, showing the riometer absorption for the beam overhead of Halley also includes a third line showing the absorptions calculated using the SIC model with no rigidity cutoffs (mid-gray line). A black bar marks the time period where the  $K_p$  conditions are most disturbed in all the panels. As there are minimal differences between the neutral atmospheres above the three beam locations, the absorptions determined for the overhead beam without considering rigidity cutoff changes will also apply for the equatorward to poleward beams. Clearly, the absorptions calculated with rigidity cutoffs are more like the experimentally observed absorptions than the case where rigidity cutoffs are not included in the model.

This figure shows that generally the absorptions calculated including the effects of the dynamic geomagnetic rigidity cutoffs (Section 2.2) are lower than those found for the no-cutoff case. This is expected, as the cutoff removes the flux of protons below the cutoff energy. However, around the time when  $K_p$  reaches  $\sim 9$  (from +48-54 hours after 0UT 4 November 2001) the absorptions in Figure 7 (mid-panel), without including rigidity cutoffs, become slightly smaller than the case where the cutoff energies have been applied. This is clearly puzzling. At these times the rigidity cutoff energies are zero (Figure 5), such that exactly the same fluxes of protons are included in the two simulations. The small difference results from ionospheric chemistry between the two runs. In the no-cutoff case, equilibrium has developed between electrons, which contribute strongly to the CNA, and negative ions, which do not. In the cutoff case, the proton fluxes suddenly increase when the cutoff threshold energy drops to zero, driven by the 3-hourly  $K_p$

values, causing a large amount of additional ionization to be produced instantaneously as electrons. Over a relatively short time period the electron and negative ion populations move into the same equilibrium as exists in the no-cutoff case, but not before which the cutoff calculations produce higher absorptions than the no-cutoff case. The same effect exists for the equatorward and poleward beams, and in both of these cases the maximum CNA at +48 hours is slightly larger than the no-cutoff case (not shown). This is primarily an artifact of the sudden change (i.e., step function) in cutoff energies imposed by the 3-hourly  $K_p$  values.

In general, the CNA estimates including the effect of changing rigidity cutoffs are fairly close to those experimentally observed. The agreement is better for the poleward and overhead observations, and worst for the most equatorward comparisons. The agreement is particularly poor for periods of the highest  $K_p$ , where the predicted absorptions are substantially higher than those observed. We find that the  $K_p$  dependent geomagnetic rigidity cutoffs do a reasonable job of predicting the SPE fluxes overhead and equatorwards of Halley for  $K_p < 5$ , but not for higher disturbance levels. At these times larger absorptions are predicted than observed experimentally, which suggests that the modeled cutoff threshold drops to lower levels than actually occurred.

The discrepancy at the highest  $K_p$  values between rigidity modeling and the observed riometer data during that period suggests that there is a problem either with the SIC calculations or the rigidity modeling. We can be confident that the SIC-model is well suited to calculating riometer absorptions during SPE when there are no significant rigidity cutoffs. Not only was the model developed for this situation, and has been successfully applied in the past [e.g., *Turunen*, 1993], the no-cutoff absorptions shown in Figure 3 (black digits in the right panel) show the linear relationship reported by *Kavanagh et al.* [2004]. For this reason we need to re-visit the rigidity cutoff energy modeling. This is examined in greater detail below.

During the SPE, the high proton fluxes will cause the altitude of peak riometer absorption to decrease in a dynamic way throughout the event. The CNA calculated from the SIC calculations

indicates that the peak absorption altitude is  $\sim 65\text{-}70$  km at the times of the maximum proton fluxes in this event. However, the changing peak absorption altitude will cause the IRIS outer beams to measure closer to the center beam during the maximum proton fluxes. At these times the poleward beam would experience lower fluxes due to rigidity, and the equatorward beam would have higher fluxes. For a fixed but high  $K_p$  levels, our Figure 7 shows that the SIC model absorption changes by 3-4 dB per degree of latitude. Thus if the beam moves towards the centre by  $\sim 0.2\text{-}0.3$  degrees in latitude as the altitude lowers during the event, there will be an effect of  $\sim 1$  dB in CNA due to the uncertainty of the beam altitude (and therefore position). This level of uncertainty in the CNA calculations are not sufficient to explain the discrepancy at the highest  $K_p$  values between rigidity modeling and the observed riometer data.

#### **5.2 Discrepancies in Modeling the Rigidity Cutoffs during 00-06 UT, 6 November 2001**

By trial and error, we found that a rigidity cutoff energy of  $\sim 18$  MeV applied in the SIC-model calculations for +48-54 hours after midnight 4 November 2001 lead to CNA estimates that were in good agreement with the centre IRIS beam. However, this is very different from the 0 MeV cutoff predicted from Figure 4 (i.e., no cutoff energy), to be contrasted with the 'crosshair' mark showing the rigidity cutoff energy required to reproduce the IRIS observations for Halley's IGRF  $L$ -value and 450 km altitude. Note that  $\sim 13$  MeV at 450 km, as shown in Figure 4, is equivalent to  $\sim 18$  MeV at 100 km. In this time period the *Smart and Shea* [2003a] modeling has lead to much smaller cutoffs than suggested by the experimental evidence, although only for very disturbed ( $K_p > 5$ ) conditions.

As noted above, the cutoff energy has been determined from the  $K_p$ -dependent Tsyganenko-89 model. However,  $K_p$  provides an indication of the global planetary disturbance levels from a limited number of ground-based sites, and as such may not represent local disturbance levels above Halley, particularly during geomagnetic storms when the variability is expected to be

extremely large. One interpretation of the differences in calculated and observed absorptions is that the riometer data are still responding to changes of the total proton flux during the early hours of 6 November (from +48 hours), but with absorption levels equivalent to local rigidity cutoff energies more appropriate for  $K_p$  values of 5-6 rather than 8-9. For this reason, we examined the observations of the Halley magnetometer for 4-8 Nov 2001, in order to estimate a local  $K$ -value. From this it appears that the Halley region was experiencing much the same disturbance-levels described by  $K_p$  (not shown), although the  $K=8$  period is shorter ( $\sim 3$  hours rather than 6), and quickly returns to  $K=5$  levels (within  $\sim 9$  hours of the beginning of the very high  $K_p$  period). Thus the difference between local  $K$  and  $K_p$  is not responsible for the differences in absorption levels during hours 48-54 (6th Nov).

It was also noted by *Smart and Shea* [2003a] that the original Tsyganenko-89 model, which they employed in their rigidity energy cutoff calculations, was valid for  $0 < K_p < 5$ , and they included the extension introduced by *Boberg* [1995], which is non-linear at higher  $K_p$  values. As the agreement between the calculations and observations is worst for  $K_p$ -values in the model extension, we have tested a linear extension of the Tsyganenko-89 model, based on the behavior from  $0 < K_p < 5$ . However, this rather arbitrary change still leads to significant over-estimates in the calculated absorption when compared with the IRIS observations (not shown). As such, this approach was not developed in more detail.

During the period of very high  $K_p$  on 6 November the observed absorption on the equatorward beam decreases, rather than increasing as predicted by the modeling. This suggests that the rigidity cutoff modeling provided by the Tsyganenko model is over-estimating the geomagnetic field distortion for these geomagnetic disturbance levels. This is also true for the central beam. However, the poleward beam does show an increase in absorption during the high  $K_p$  period. We initially tested the idea that for the highest  $K_p$  levels, we could simulate a less distorted field by shifting the latitudes of all three beam locations equatorwards. In order to force the centre beam

cutoff energies to be correct, we needed to shift the beam location by  $8.5^\circ$  in latitude equatorwards for the period when  $K_p > 5$ . This approach did produce reasonable agreement between the calculated and expected cutoff energies for all three beams, providing strong evidence that the geomagnetic field is less distorted at these times than the Tsyganenko model employed by *Smart and Shea* [2003a] might suggest. However, this is clearly an extreme shift, and while sufficient to show that the field is considerably less stretched, it is not well suited for providing predictions of rigidity energy cutoffs with varying geomagnetic disturbance levels. Our analysis suggests that the rigidity energy cutoffs provided by *Smart and Shea* [2003a] work well in conditions of low to mid geomagnetic disturbance levels, i.e.,  $K_p \leq 5$ . In more disturbed conditions the rigidity energy cutoffs indicated by the IRIS observations appear to saturate around those predicted for  $K_p \approx 6$ . This suggests that the geomagnetic latitude limit for the penetration of SPE protons during large geomagnetic storms is rather more poleward than has been indicated previously, except for the highest proton energies which can penetrate to very low geomagnetic latitudes (Figure 4).

## 6. Global Rigidity Cutoff Maps

The plot of effective vertical cutoff energies against geomagnetic latitude varying with geomagnetic activity (Figure 4) is useful for summarizing the response of the geomagnetic field during geomagnetic storms. However, it is also useful to consider the geographic variation in geomagnetic rigidity cutoffs, so as to determine the size of atmospheric regions which will be affected during SPEs. Figure 8 presents maps of the proton geomagnetic rigidity cutoff energies for the southern and northern hemispheres at very low ( $K_p=0$ ), mid ( $K_p=4$ ) and high ( $K_p=9$ ) disturbance levels, based on the conclusions outlined Section 5. Contour lines with units of MeV mark the geographic locations of the rigidity cutoff energies at 100 km altitude. Note that the location of the cutoffs for  $K_p=0$  and  $K_p=4$  are simply projected from Figure 4, and thus are based

on the Tsyganenko-89 magnetic field model. For the lower panels of Figure 8, we have made use of our conclusions from Section 5.2, and have taken the rigidity cutoff energies for this very disturbed situation to be represented by the  $K_p=6$  line in Figure 4.

During geomagnetic storms, SPE particles impact larger regions of the polar atmosphere. The contour line in Figure 8 showing the cutoff location for an energy of 1 keV (=0.001 MeV) is indicative of the 'no-cutoff' region; essentially all SPE particles will access the upper atmosphere located polewards of this line, irrespective of the particle energy. As shown in this figure, the size of the 'no-cutoff' region expands significantly equatorwards with geomagnetic activity. The ionization in the ionospheric D region (and below) is mainly caused by protons with energies in the range of 1-100 MeV, corresponding to altitudes ranging over about 80-30 km respectively. Outside of the 100 MeV contour, little ionospheric changes will occur, and subionospheric radio wave propagation equatorward of this contour should be essentially unaffected. However, SPE particles with even greater energies (>500 MeV) can reach the surface of the Earth, producing Ground Level Enhancements in cosmic ray detectors. Figure 8 shows that the locations of the rigidity cutoffs for these high energies are not as strongly dependent upon the level of geomagnetic disturbance as the low energy case. Note that experimental measurements on this scale are extremely rare at this stage. However, the basic shape of the SPE affected region predicted by our modelling (Figure 8) is rather similar to the zone of high ozone losses observed by satellite measurements during an SPE event [Seppälä *et al.*, 2004].

It has been shown that there is an empirical relationship between the square root of the integral proton flux (>10 MeV) and riometers cosmic noise absorption (CNA) in daytime, at least when geomagnetic cutoff effects do not limit the fluxes [Kavanagh *et al.*, 2004]. This relationship might be used to deduce the >10 MeV integral proton flux levels from riometer measurements, independent of GOES observations. However, a more useful application would be the identification of additional energy inputs beyond the SPE particles, where the riometers

absorptions were larger than those predicted from the empirical relationship. However, some care needs to be taken with the application of this empirical relationship. As is clear from the Halley IRIS data (Figure 3), not all riometer absorptions will be well described by this relationship. The 10 MeV contour line in Figure 8 provides an indication of riometer locations for which this relationship should hold, and how these locations will vary with geomagnetic disturbance levels.

## 7. Discussion

The Tsyganenko geomagnetic field models are amongst a small set of external field models which are commonly used as standard tools throughout the community. However, it is less widely appreciated that at highly disturbed geomagnetic conditions all geomagnetic field models struggle to reproduce the experimentally observed fields. Figure 9 shows the  $L$ -value of Halley calculated using various field models during the 4 November 2001 SPE event, to be contrasted against the IGRF and Tsyganenko-89 magnetic field models which are the basis of the rigidity cutoff energy predictions. The additional  $L$ -value calculations shown in the figure were undertaken using the European Space Agency's Space Environment Information System (SPENVIS), taking as input 3-hourly geophysical parameters (geomagnetic indices, solarwind and IMF measurements) provided by the NSSDC OMNIWeb databases. The three-hour time scale is to provide 'like with like' comparison with the  $K_p$ -driven Tsyganenko-89 model. Figure 9 includes the Ostapenko-Maltsev [Ostapenko and Maltsev, 1997], Olson-Pfitzer dynamic [Pfitzer *et al.*, 1988], Tsyganenko96 [Tsyganenko, 1996] and "Parabaloid" magnetic field models, the last of which has been proposed as ISO standard for the Earth's Magnetospheric magnetic field and has been developed jointly by research teams from the Skobeltsyn Institute of Nuclear Physics and the U. S. Geological Survey as described on SPENVIS. Note that there is a large data gap in Figure 9, covering hours 51-75. This is due to a gap in solar wind/IMF measurements, required

as inputs for all the additional magnetic field models. This gap starts just after the beginning of the peak disturbance as measured by  $K_p$  (hours 48-54).

It is instructive to consider the wide variation in  $L$ -values reported for Halley by the differing magnetic field models during the 4-7 November 2001 storm period (Figure 9). We argued in Section 5 that the IRIS absorption measurements indicate that the geomagnetic field is not as stretched at high  $K_p$  as suggested by the Tsyganenko-89 field model, and that while Halley should effectively move polewards in  $L$ -value during this period, the shift should be reasonably slight. From the observed absorption levels it appears that at the peak storm time of 4-7 November 2001, the geomagnetic field was distorted such that Halley moved polewards only by about  $\Delta L=1$ . The Tsyganenko-89 model suggests that the  $L$ -value of Halley is shifted to  $L\approx 6.5$  (i.e.,  $\Delta L\approx 2$ ). The rigidity cutoff energy of  $\approx 18$  MeV for highly disturbed conditions is consistent with an IGRF L-shell of  $L=5.5$  ( $\approx 3.5^\circ$  poleward of Halley) during low disturbance conditions (e.g.,  $K_p \approx 1$ ). However, Figure 9 indicates that the Tsyganenko-89 model is relatively conservative when contrasted with the Tsyganenko-96 and Olson-Pfizer dynamic calculations, which lead to much larger polewards shifts ( $\Delta L > 6$  and  $\Delta L \approx 4$ , respectively), and very low values of rigidity cutoff energy. In contrast, the Ostapenko-Maltsev and Parabaloid magnetic field models report smaller shifts in  $L$ -value during these storm conditions, both reaching  $L \approx 5.5$  around the time of the highest  $K_p$  values, and thus a rigidity cutoff energy of about 18 MeV as determined above. Although further tests would be valuable, it appears these dynamic magnetic field models would be good candidates for future work into time-varying rigidity cutoff energies, following the approach of Smart and Shea.

## 8. Summary

SPEs are major, though infrequent, space weather phenomena that can produce hazardous effects in the near-Earth space environment. A detailed understanding of their effects depends

upon knowledge of the dynamic rigidity cutoffs imposed by the changing total magnetic field. Recently, dynamic vertical cutoff rigidities have been determined for SPE protons [*Smart and Shea, 2001*], using the magnetic-activity level dependent Tsyganenko magnetospheric field model [*Tsyganenko, 1989*]. In this paper we have undertaken a detailed case study of the 4-10 November 2001 SPE, contrasting the varying, predicted and observed, rigidity cutoffs during a large geomagnetic disturbance. Ground-based measurements are provided by an imaging riometer at Halley Bay, Antarctica, fortunately situated such that the rigidity cutoff sweeps back and forth across the instrument's field of view during the SPE period.

The  $K_p$ -dependent geomagnetic rigidity cutoff energies have been determined from SAMPEX observations and the particle-tracing of Smart and Shea based on the Tsyganenko-89 magnetic field model. These have been taken as energy cutoffs on satellite derived proton fluxes, which have been used to calculate the predicted cosmic noise absorption levels for the Halley IRIS riometer during this SPE event. We find that the predicted absorption levels show good agreement with those experimentally observed for low and mid levels of geomagnetic disturbance levels ( $K_p < 5$ ). However, during more disturbed geomagnetic conditions the Smart and Shea modeling over-estimates the stretching of the geomagnetic field, under-estimating the rigidity cutoff energies, and hence leading to absorption predictions that are too high. In very disturbed conditions ( $K_p \approx 7-9$ ) the rigidity energy cutoffs indicated by the IRIS observations appear to saturate around those predicted for  $K_p \approx 6$  by the particle-tracing approach. This suggests that the geomagnetic latitude limit for the penetration of SPE protons during large geomagnetic storms is rather more poleward than has been indicated previously, except for the highest proton energies which can penetrate to very low geomagnetic latitudes. Examples of the changing rigidity cutoff contours for increasing levels of geomagnetic disturbance have been presented as maps for the northern and southern hemisphere.

While the Tysganenko-89 magnetic field model over-estimates the geomagnetic field distortion for very high  $K_p$ , some other magnetic field models suggest either higher or lower distortion levels for the conditions during this storm. It appears that the Ostapenko-Maltsev and Parabaloid dynamic magnetic field models would be good candidates for future work into time-varying rigidity cutoffs through particle-tracing.

**Acknowledgments.** C.J.R. would like to thank Allison H. Franklin of Napier for her support. The Halley IRIS system was supported in part by a grant from the National Science Foundation to the University of Maryland We are grateful for the online model and data repositories provided by the SPENVIS, SPIDR, and OmniWEB services.

## References

- Bailey, D. K., Disturbances in the lower ionosphere observed at VHF following the solar flare of 23 February 1956 with particular reference to the auroral zone absorption, *J Geophys. Res.*, 62, 431-463, 1957.
- Banks, P. M., and G. Kockarts, *Aeronomy*, vol. B, chap. 15, Academic Press, 1973.
- Boberg, P. R. Jr., E. O. Flückiger, and E. Kobel, Geomagnetic transmission of solar energetic protons during the geomagnetic disturbances of October 1989, *Geophys. Res. Lett.*, 22(9), 1133-1136, 10.1029/95GL00948, 1995.
- Brasseur, G., and S. Solomon, *Aeronomy of the Middle Atmosphere*, second ed., D. Reidel Publishing Company, Dordrecht, 1986.
- Cane H. V., T. T. von Roseninge, C. M. S. Cohen, and R. A. Mewaldt, Two components in major solar particle events, *Geophys. Res. Lett.*, 30(12), 8017, doi:10.1029/2002GL016580, 2003.

- Chabrillat, S., G. Kockarts, D. Fonteyn, and G. Brasseur, Impact of molecular diffusion on the CO<sub>2</sub> distribution and the temperature in the mesosphere, *Geophys. Res. Lett.*, 29, 1-4, 2002.
- Clilverd, M. A., C. J. Rodger, Th. Ulich, A. Seppälä, E. Turunen, A. Botman, and N. R. Thomson, Modeling a large solar proton event in the southern polar cap, *J. Geophys. Res.*, 110, A09307, doi:10.1029/2004JA010922, 2005a.
- Clilverd, M. A., A. Seppälä, C. J. Rodger, N. R. Thomson, P. T. Verronen, E. Turunen, Th. Ulich, J. Lichtenberger, and P. Steinbach, Modeling the ionospheric effects of solar proton events in the polar atmosphere, *Radio Sci.*, (in review), 2005b.
- Detrick, D. L., and T. J. Rosenberg: A phased-array radio wave imager for studies of cosmic noise absorption, *Radio Sci.*, 325-338, 1990.
- Dyer, C. S., and F. Lei, S. N. Clucas, D. F. Smart, and M. A. Shea, Calculations and observations of solar particle enhancements to the radiation environment at aircraft altitudes, *Adv. Space Res.*, 32(1), 81-93, 2003.
- Fanselow, J. L., and E. C. Stone, Geomagnetic cutoffs for cosmic-ray protons for 7 energy intervals between 1.2 and 39 MeV, *J. Geophys. Res.*, 77(22), 3999, 1972.
- Hargreaves, J. K., *The solar-terrestrial environment*, Atmospheric and Space Science Series, Cambridge University Press, Cambridge, UK, 1992.
- Hargreaves, J. K., and M. J. Jarvis, The multiple riometer system at Halley, Antarctica, *British Antarctic Surv. Bull.*, 72, 13-23, 1986.
- Hedin, A. E., Extension of the MSIS Thermospheric model into the middle and lower Atmosphere, *J. Geophys. Res.*, 96, 1159-1172, 1991.
- Jarvis M. J., R. E. Hibbins, M. J. Taylor, T. J. Rosenberg, Utilizing riometry to observe gravity waves in the sunlit mesosphere, *Geophys. Res. Lett.*, 30 (19), 1979, doi:10.1029/2003GL017885, 2003.

- Kavanagh, A. J., S. R. Marple, F. Honary, I. W. McCrea, and A. Senior, On solar protons and polar cap absorption: constraints on an empirical relationship, *Ann. Geophys.*, 22(4), 1133-1147, 2004.
- Kress B. T., M. K. Hudson, K. L. Perry, and P. L. Slocum, Dynamic modeling of geomagnetic cutoff for the 23–24 November 2001 solar energetic particle event, *Geophys. Res. Lett.*, 31, L04808, doi:10.1029/2003GL018599, 2004.
- Krishnaswamy, S., D. L. Detrick, and T. J. Rosenberg, The inflection point method of determining riometer quiet day curves, *Radio Sci.*, 20, 123-136, 1985.
- Krucker, S., and R. P. Lin, Two classes of solar proton events derived from onset time analysis, *Astrophys. J.*, 542(1): 61-64, 2000.
- Little, C. G, and H. Leinbach, The riometer - a device for the continuous measurement of ionospheric absorption, *Proceedings of the IRE*, 47, 315-319, 1959.
- Ogliore, R. C., R. A. Mewaldt, R. A. Leske, E. C. Stone, and T. T. von Rosenvinge, A direct measurement of the geomagnetic cutoff for cosmic rays at space station latitudes, *Proceedings of ICRC 2001*, 4112-4115, Copernicus Gesellschaft, 2001.
- Ostapenko, A. A., and Y. P. Maltsev, Relation of the magnetic field in the magnetosphere to the geomagnetic and solar wind activity, *J. Geophys. Res.*, 102, 17467-17473, 1997.
- Pfizer, K. A., W. P. Olson, and T. Mogstad, A time dependent source driven magnetospheric magnetic field model, *EOS Trans.*, 69, 426, 1988.
- Randall C. E., V. L. Harvey, G. L. Manney, Y. Orsolini, M. Codrescu, C. Sioris, S. Brohede, C. S. Haley, L. L. Gordley, J. M. Zawodny, and J. M. Russell, Stratospheric effects of energetic particle precipitation in 2003–2004, *Geophys. Res. Lett.*, 32, L05802, doi:10.1029/2004GL022003, 2005.
- Reeves, G. D., T. E. Cayton, S. P. Gary, and R. D. Belan, The great solar energetic particle events of 1989 observed from geosynchronous orbit, *J. Geophys. Res.*, 97, 6219-6226, 1992.

- Reid, G. C., S. Solomon, and R. R. Garcia, Response of the middle atmosphere to solar proton events of August-December, 1989, *Geophys. Res. Lett.*, 18, 1019-1022, 1991.
- Rose, M. C., M. J. Jarvis, M. A. Clilverd, D. J. Maxfield, and T. J. Rosenberg, The effect of snow accumulation on imaging riometer performance, *Radio Sci.*, 35, 1143-1153, 2000.
- Selesnick, R. S., A. C. Cummings, J. R. Cummings, R. A. Mewaldt, E. C. Stone, and T. T. von Rosenvinge, Geomagnetically trapped anomalous cosmic rays, *J. Geophys. Res.*, 100, 9503-9518, 1995.
- Sen, H. K., and A. A. Wyller, On the generalization of the Appleton-Hartree magnetoionic formulas, *J. Geophys. Res.*, 65, 3931-3950, 1960.
- Seppälä, A., P. T. Verronen, E. Kyrölä, S. Hassinen, L. Backman, A. Hauchecorne, J. L. Bertaux, and D. Fussen, Solar Proton Events of October-November 2003: Ozone depletion in the Northern hemisphere polar winter as seen by GOMOS/Envisat, *Geophys. Res. Lett.*, 31(19), L19,107, doi:10.1029/2004GL021042, 2004.
- Shea, M. A., and D. F. Smart, A summary of major solar proton events, *Solar Phys.*, 127(2), 297-320, 1990.
- Shimazaki, T., *Minor Constituents in the Middle Atmosphere (Developments in Earth and Planetary Physics, No 6)*, D. Reidel Publishing Co., Dordrecht, Netherlands, 1984.
- Smart, D. F., and M. A. Shea, Geomagnetic cutoffs - a review for space dosimetry applications, *Adv. Space Res.*, 14(10), 787-796, 1994.
- Smart, D. F., and M. A. Shea, A simplified model for timing the arrival of solar flare-initiated shocks, *J. Geophys. Res.*, 90, 183-190, 1985.
- Smart, D. F., and M. A. Shea, Comparison of the Tsyganenko model predicted and measured geomagnetic cutoff latitudes, *Adv. Space Res.*, 28(12), 1733-1738, 2001.
- Smart, D. F., and M. A. Shea, The space developed dynamic vertical cutoff and its applicability to aircraft radiation dose, *Adv. Space Res.*, 32(1), 103-108, 2003a.

- Smart, D. F., and M. A. Shea, Geomagnetic cutoff rigidity calculations at 50-year intervals between 1600 and 2000, *Proc. ICRC 2003*, 4201-4204, Universal, 2003b.
- Smart, D. F., M. A. Shea, M. J. Golightly, M. Weyland, and A. S. Johnson, Evaluation of the dynamic cutoff rigidity model using dosimetry data from the STS-28 flight, *Adv. Space Res.*, 31(4), 841-846, 2003.
- Stauning, P., Ionospheric investigations using imaging riometer observations, in *Review of Radio Science 1993-1996*, edited by W. R. Stone, pp. 157-161, Oxford Univ. Press, Oxford, England, 1996.
- Störmer, C., Periodische Elektronenbahnen im Feld eines Elementarmagnetron und ihre Anwendung auf Bruches Modellversuche und auf Eschenhagens Elementarwellen des Erdmagnetismus, *Zeitschr. f. Astrophys.*, 1, 237-274, 1930.
- Thomas, L., and M. R. Bowman, A study of pre-sunrise changes in negative ions and electrons in the D-region, *J. Atmos. Terr. Phys.*, 4, 219, 1986.
- Tobiska, W. K., T. Woods, F. Eparvier, R. Viereck, L. D. B. Floyd, G. Rottman, and O. R. White, The SOLAR2000 empirical solar irradiance model and forecast tool, *J. Atmos. Terr. Phys.*, 62, 1233-1250, 2000
- Tsyganenko, N. A., Determination of magnetospheric current system parameters and development of experimental geomagnetic models based on data from IMP and HEOS satellites, *Planet. Space Sci.*, 37, 5-20, 1989.
- Tsyganenko, N. A., Effects of the solar wind conditions on the global magnetospheric configuration as deduced from data-based field models, Proc. 3rd International Conference on Substorms (ICS-3), Versailles, France, 12-17 May 1996, ESA SP-389, 181-185, 1996.
- Turunen E., EISCAT incoherent scatter radar observations and model studies of day to twilight variations in the D region during the PCA event of August, 1989, *J. Atmos. Terr. Phys.*, 55(4-5), 767-781, 1993.

Turunen, E., H. Matveinen, J. Tolvanen, and H. Ranta, D-region ion chemistry model, in *STEP Handbook of Ionospheric Models*, edited by R. W. Schunk, pp. 1-25, SCOSTEP Secretariat, Boulder, Colorado, USA, 1996.

Verronen, P. T., E. Turunen, Th. Ulich, and E. Kyrölä, Modelling the effects of the October 1989 solar proton event on mesospheric odd nitrogen using a detailed ion and neutral chemistry model, *Ann. Geophys.*, 20, 1967-1976, 2002.

Verronen, P. T., A. Seppälä, M. A. Clilverd, C. J. Rodger, E. Kyrölä, C.-F. Enell, Th. Ulich, and E. Turunen, Diurnal variation of ozone depletion during the October-November 2003 solar proton event, *J. Geophys. Res.*, 110(A9), doi:10.1029/2004JA010932, 2005.

Westerlund, S., F. H. Reeder, and C. Abom, Effects of polar cap absorption events on VLF transmissions, *Planet. Space Sci.*, 17, 1329-1374, 1969.

---

M. A. Clilverd and M. J. Jarvis, Physical Sciences Division, British Antarctic Survey, High Cross, Madingley Road, Cambridge CB3 0ET, England, U.K. (e-mail: M.Clilverd@bas.ac.uk; M.Jarvis@bas.ac.uk)

C. J. Rodger, Department of Physics, University of Otago, P.O. Box 56, Dunedin, New Zealand. (email: crodger@physics.otago.ac.nz).

E. Turunen and Th. Ulich, Sodankylä Geophysical Observatory, Tähteläntie 62, FIN-99600 Sodankylä, Finland. (email: esa@sgo.fi, thu@sgo.fi).

P. T. Verronen, Earth Observation, Finnish Meteorological Institute, P.O. Box 503 (Vuorikatu 15 A), FIN-00101 Helsinki, Finland. (email: pekka.verronen@fmi.fi).

RODGER ET AL.: RIOMETER ESTIMATED RIGIDITY CUTOFFS

**Figure 1.** Geospace conditions during the 4-10 November 2001 Solar Proton Events. The upper panel shows integral unidirectional proton flux measurements reported by the geostationary GOES-8 satellite. The lower panel shows the 3-hourly  $K_p$  geomagnetic disturbance levels for the same time period.

**Figure 2.** Map showing the region in Antarctica in which our study is undertaken. The square marks the location of the Halley IRIS riometers ( $75.6^\circ\text{S}$ ,  $26.32^\circ\text{W}$ ,  $L=4.6$ ).

**Figure 3.** Experimentally-observed IRIS cosmic noise absorptions (after the removal of the QDC) reported during the 4-10 November 2001 SPE from Halley, Antarctica. The left panel shows the variation of the CNA with time. The right panel shows the same absorptions, but testing the relationship between CNA and proton flux, where the numbers represents the  $K_p$  at that time. In this panel the black digits are calculated for a no-rigidity cutoff case, while the red, blue and green numbers represent the equatorward, mid, and poleward beams.

**Figure 4.** Variation with geomagnetic activity of the effective vertical cutoff energies for protons at an altitude of 450 km, based on the modeling of *Smart et al.* [2003] and SAMPEX observations [*Ogliore et al.*, 2001].

**Figure 5.** Time varying geomagnetic cutoff energy determined from the model, as described in section 4.2. Note the large differences in cutoff energy for the poleward and equatorward IRIS beams, located only  $\sim 2^\circ$  apart in latitude.

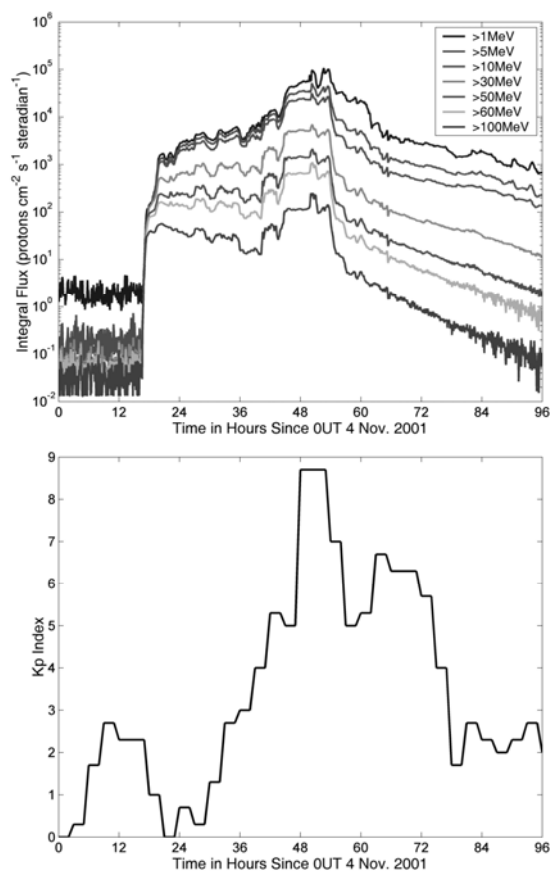
**Figure 6.** Response of the electron number density of the middle atmosphere to the 4-10 November 2001 SPE event (SIC modeling results). A white bar marks the time period where the  $K_p$  conditions are most disturbed. The upper most panel shows the expected electron density directly overhead of Halley for a no-rigidity cutoff case. The second panel shows the electron density for the same location when the fluxes are cutoff by the varying geomagnetic cutoffs show in Figure 4. The lower two panels show the ratio of the electron densities of the

equatorward and poleward IRIS beams to the overhead (middle beam) electron densities shown in the second panel.

**Figure 7.** Comparison between the experimentally observed and calculated cosmic noise absorption for the Halley IRIS instrument for the range of beam directions. The plots show the observed CNA (heavy black line), the predicted CNA with geomagnetic rigidity cutoffs (light gray line), and the predicted CNA without cutoffs applied (mid-gray line, middle panel only). A black bar marks the time period where the  $K_p$  conditions are most disturbed.

**Figure 8.** Contour plots showing the locations of the rigidity energy cutoffs at 100 km predicted from our study. The contour labels have units of MeV, and the location Halley is shown with a square. Note that as the geomagnetic activity levels increase, the cutoffs move equatorward.

**Figure 9** Comparison of the McIlwain  $L$ -value determined by various geomagnetic field models. The IGRF internal field (dotted), and the  $K_p$ -dependent Tsyganenko-89 model (solid) used in this study, are contrasted against a number of differing 'standard' models.

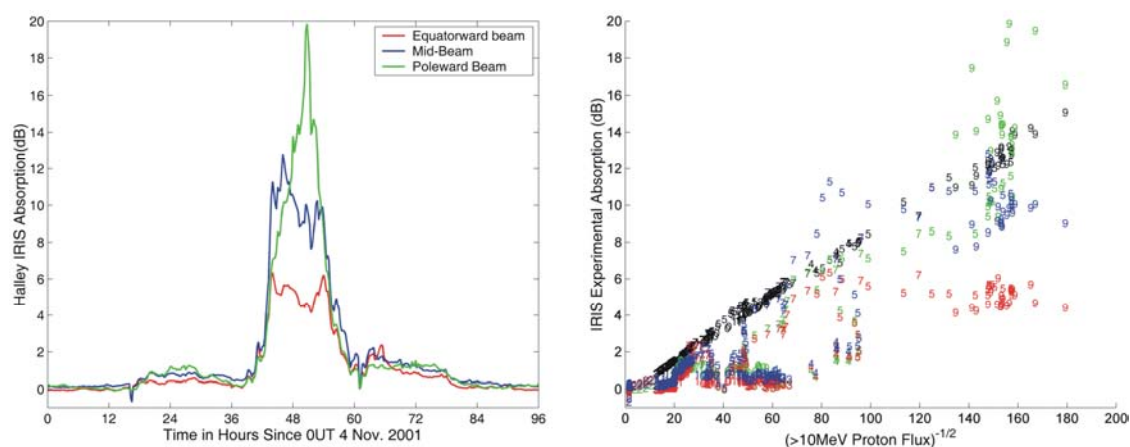
**F1**

**Figure 1.** Geospace conditions during the 4-10 November 2001 Solar Proton Events. The upper panel shows integral unidirectional proton flux measurements reported by the geostationary GOES-8 satellite. The lower panel shows the 3-hourly  $K_p$  geomagnetic disturbance levels for the same time period.



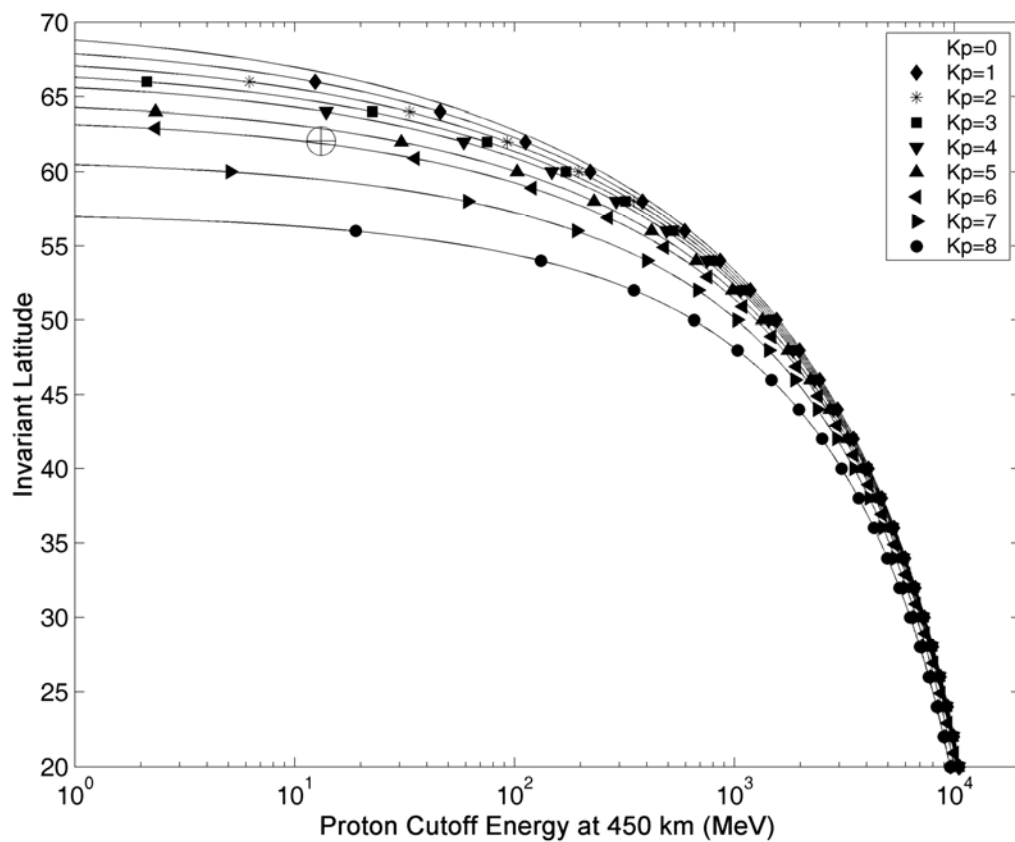
F2

**Figure 2.** Map showing the region in Antarctica in which our study is undertaken. The square marks the location of the Halley IRIS riometers ( $75.6^{\circ}\text{S}$ ,  $26.32^{\circ}\text{W}$ ,  $L=4.6$ ).



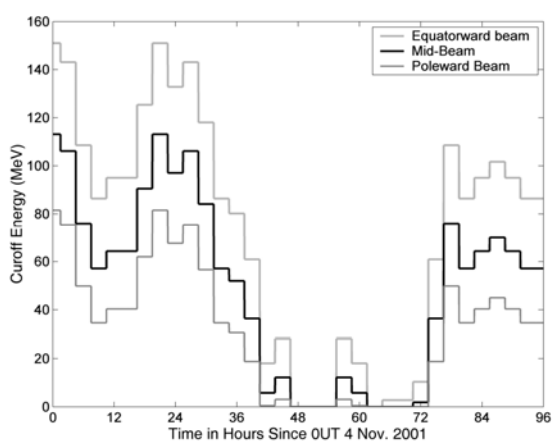
F3

**Figure 3.** Experimentally-observed IRIS cosmic noise absorptions (after the removal of the QDC) reported during the 4-10 November 2001 SPE from Halley, Antarctica. The left panel shows the variation of the CNA with time. The right panel shows the same absorptions, but testing the relationship between CNA and proton flux, where the numbers represents the  $K_p$  at that time. In this panel the black digits are calculated for a no-rigidity cutoff case, while the red, blue and green numbers represent the equatorward, mid, and poleward beams.



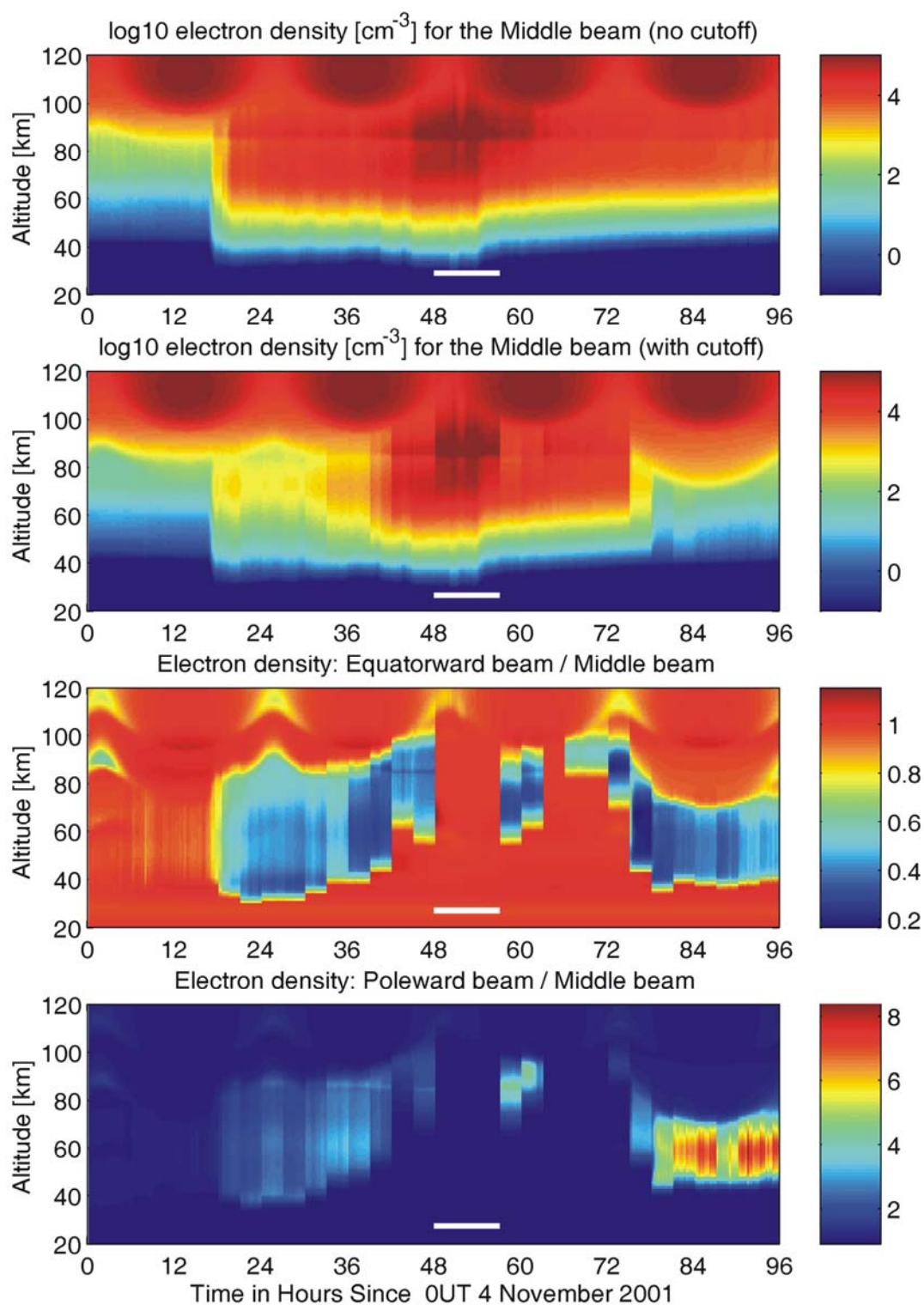
F4

**Figure 4.** Variation with geomagnetic activity of the effective vertical cutoff energies for protons at an altitude of 450 km, based on the modeling of *Smart et al.* [2003] and SAMPEX observations [*Ogliore et al.*, 2001].



F5

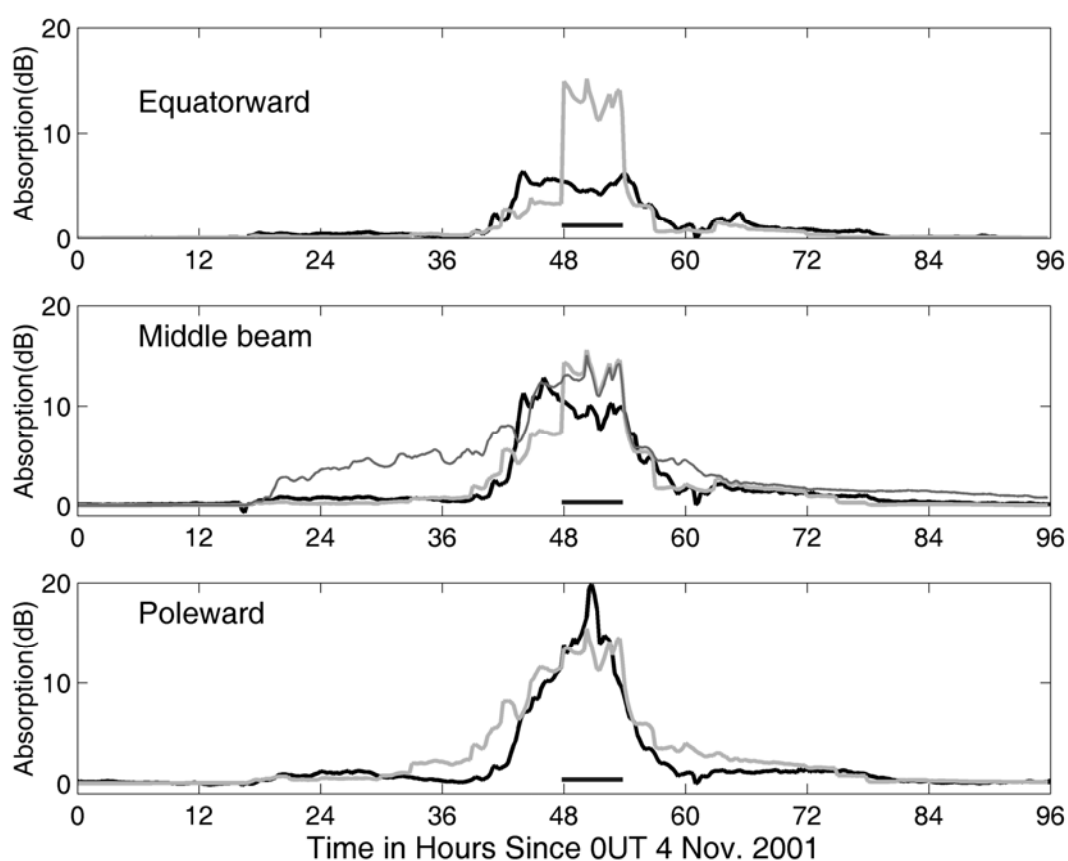
**Figure 5.** Time varying geomagnetic cutoff energy determined from the model, as described in section 4.2. Note the large differences in cutoff energy for the poleward and equatorward IRIS beams, located only  $\sim 2^\circ$  apart in latitude.



F6

**Figure 6.** Response of the electron number density of the middle atmosphere to the 4-10 November 2001 SPE event (SIC modeling results). A white bar marks the time period where the

$K_p$  conditions are most disturbed. The upper most panel shows the expected electron density directly overhead of Halley for a no-rigidity cutoff case. The second panel shows the electron density for the same location when the fluxes are cutoff by the varying geomagnetic cutoffs show in Figure 4. The lower two panels show the ratio of the electron densities of the equatorward and poleward IRIS beams to the overhead (middle beam) electron densities shown in the second panel.

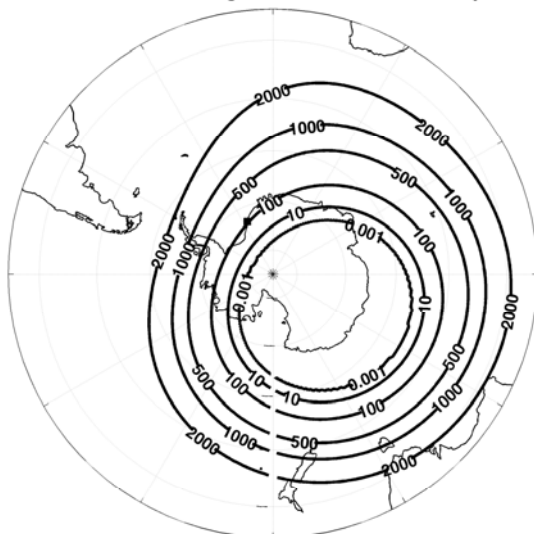


F7

**Figure 7.** Comparison between the experimentally observed and calculated cosmic noise absorption for the Halley IRIS instrument for the range of beam directions. The plots show the observed CNA (heavy black line), the predicted CNA with geomagnetic rigidity cutoffs (light

gray line), and the predicted CNA without cutoffs applied (mid-gray line, middle panel only). A black bar marks the time period where the  $K_p$  conditions are most disturbed.

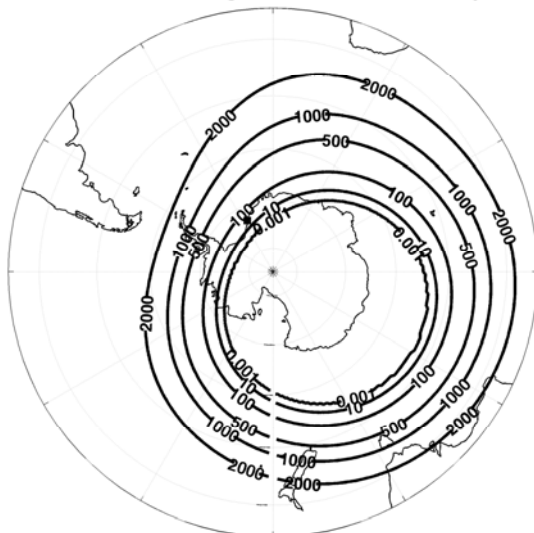
Proton Cutoff Energies at 100km altitude: Kp=0



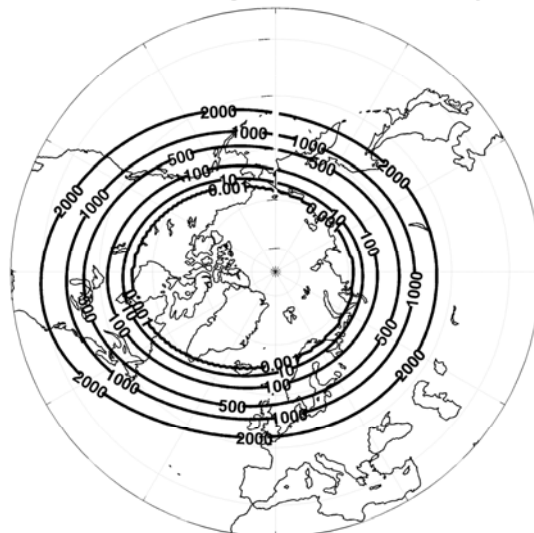
Proton Cutoff Energies at 100km altitude: Kp=0



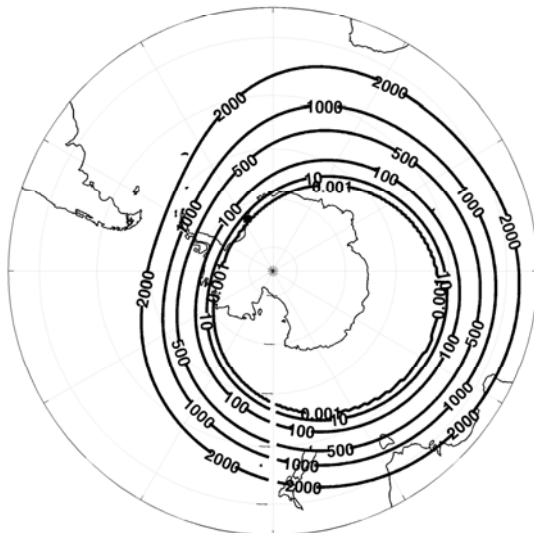
Proton Cutoff Energies at 100km altitude: Kp=4



Proton Cutoff Energies at 100km altitude: Kp=4



Proton Cutoff Energies at 100km altitude: Kp=9



Proton Cutoff Energies at 100km altitude: Kp=9

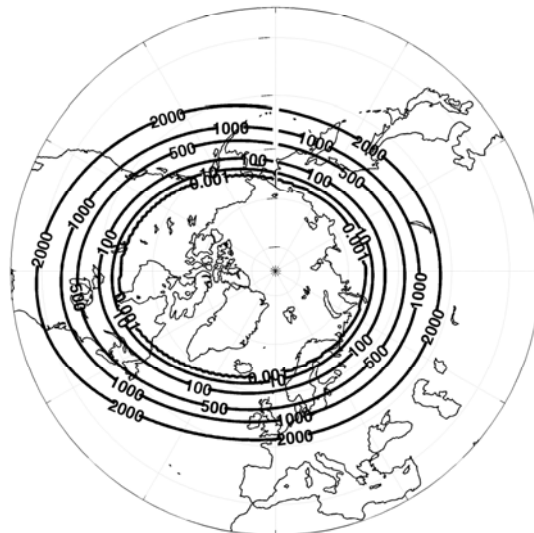
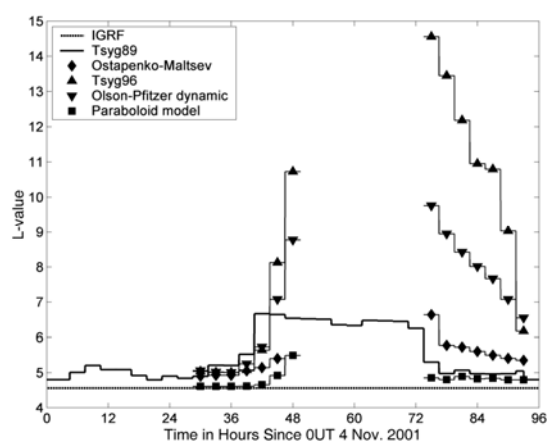


**Figure 8.** Contour plots showing the locations of the rigidity energy cutoffs at 100 km predicted from our study. The contour labels have units of MeV, and the location Halley is shown with a square. Note that as the geomagnetic activity levels increase, the cutoffs move equatorward.



F9

**Figure 9** Comparison of the McIlwain  $L$ -value determined by various geomagnetic field models. The IGRF internal field (dotted), and the  $K_p$ -dependent Tsyganenko-89 model (solid) used in this study, are contrasted against a number of differing 'standard' models.